Journal Name

ARTICLE

Comparison of tetrel bonds in neutral and protonated complexes of pyridineTF_3 and furanTF_3 (T = C, Si, and Ge) with NH_3

Mingxiu Liu[a], Qingzhong Li[*,a], Steve Scheiner[*,b]

fReceived 00th January 20xx,
Accepted 00th January 20xx

DOI: 10.1039/x0xx00000x

www.rsc.org/

Ab initio calculations have been performed for the complexes H^+-$PyTX_3$···NH_3 and H^+-furanTF_3···NH_3 (T = C, Si, and Ge; X = F and Cl) with focus on geometries, interaction energies, orbital interactions, and electron densities at the MP2/aug-cc-pVTZ level to study the influence of protonation on the strength of tetrel bonding. The primary interaction mode between α/β-furanCF_3/*p*-$PyCF_3$ and NH_3 changes from a F···H hydrogen bond to a C···N tetrel bond as a result of protonation. Importantly, the protonation has a prominent enhancing effect on the strength of tetrel bonding with an increase of interaction energy from 14 to 30 kcal/mol. The tetrel bonding becomes stronger in the order H^+-*p*-$PySiF_3$···NH_3<H^+-*m*-$PySiF_3$···NH_3<H^+-*o*-$PySiF_3$···NH_3, showing a reverse trend from that of the neutral analogues. In addition, there is a competition between the tetrel and hydrogen bond in the protonated complexes, in which the hydrogen bond is favored in the complexes of H^+-*p*-$PyCF_3$ but the tetrel bond is preferred in the complexes of H^+-*p*-$PyTX_3$ (T = Si, Ge; X = F, Cl) and H^+-*o*/*m*-$PySiF_3$.

1. Introduction

Noncovalent interactions, particularly hydrogen bonds, have potential applications in physics, chemistry, and biology.[1] Recently, a new type of noncovalent interaction, tetrel bonding, has received renewed interest experimentally[2-11] and theoretically,[12-34] following earlier pioneering works.[35-42] The existence of tetrel bonding in crystal materials has been confirmed by a survey of the Cambridge Structure Database (CSD).[2-4] Accordingly, tetrel bonding is expected to be an effective and reliable force in crystal engineering, supramolecular chemistry, and biochemistry.[2] The formation of tetrel bonding can be explained by the concept of a σ–hole, a region of positive electrostatic potential on a Group 14 atom surface.[12] The tetrel bond is defined the interaction between the σ–hole of the Group 14 atom and a Lewis base.[13-19] π-hole tetrel bonding has also been proposed.[20] It was demonstrated that the driving force for the observed Si-O-N angle contraction in molecules XYZSi-O-N$(CH_3)_2$ is largely the electrostatic attraction between a positive σ–hole on the silicon and the lone pair of the nitrogen.[21] An "inverse sandwich" structure formed by decachlorocyclopentasilane (Si_5Cl_{10}) with organocyanides is mainly governed by a fairly weak interaction between the Si_5 ring and the coordinative organocyanide ligands.[22] The formation of a four-centered transition complex combined with O···Si and N···Si interactions was proposed in the reaction of phenyltrifluorosilane with 2-aminoethanol and its N-methyl derivatives.[23] In addition, tetrel bonding also makes an important contribution to the formation of the preliminary stage and transition state of the S_N2 reaction.[24,25] Importantly, tetrel bonding may play a role in anion recognition[26] since chlorine-containing cyclohexasilanes can strongly bind electron-rich guests.[27] Very recently, some compounds involving Pb(II) have been used to prepare supramolecular assemblies by means of tetrel bonding and other interactions.[8-10] So, it is urgent to find more evidence for the existence of tetrel bonding in different systems including solutions, tap its potential applications in different fields (particularly biological systems), and understand its properties and factors contributing to variation of its strength.

The functions of tetrel bonding exhibit dependence on its strength. It is accepted that the strength of tetrel bonding can be tuned by changing the magnitude of the σ–hole on the Group 14 atom,[28,29] which depends on the nature of this atom and the electron-withdrawing ability of groups adjoining it. Specifically, the σ–hole on the Group 14 atom becomes more intense in the order C < Si < Ge < Sn, and stronger electron-withdrawing substituents enlarge this hole. The strength of tetrel bonding can also be affected by the cooperativity of tetrel bonding with other such bonds and other interactions.[18,43-55]

It has been demonstrated that protonation is ubiquitous and of great importance in chemical and biological systems.[56-66] For example, the protonation of DNA plays an important role in certain biochemical processes.[63] Usually, protonation is involved in the formation of a hydrogen bond. Owing to the fact that pyridine and its derivatives can be used as building blocks in crystal engineering,[67-69] they are often taken as model molecules in studying the protonation phenomenon, in which the N atom is protonated.[57-59,54-66] A prominent feature of N protonation in pyridine is an increased acidity of the C–H hydrogen atom, allowing it to form a strong hydrogen bond.[66] If the H atom of pyridine is replaced by a group such as $–TF_3$ (T = C, Si, and Ge), how does this affect the acidity and the strength of tetrel bonding?

[a] *The Laboratory of Theoretical and Computational Chemistry, School of Chemistry and Chemical Engineering, Yantai University, Yantai 264005, People's Republic of China. E-mail: liqingzhong1990@sina.com; Fax: +86 535 6902063; Tel: +86 535 6902063.*
[b] *Department of Chemistry and Biochemistry, Utah State University, Logan, UT 84322-0300, USA E-mail: steve.scheiner@usu.edu.*
†Electronic Supplementary Information (ESI) available: [Figs. S1-S7 and Tables S1-S7]. See DOI: 10.1039/x0xx00000x

To answer this question, we designed complexes of *p*-PyTF$_3$ (T = C, Si, and Ge) with NH$_3$ (Scheme 1) to study the influence of protonation on the strength of tetrel bonding. The *p*-PySiCl$_3$···NH$_3$ complex is used to study the effect of halogen. The effect of the substitution position of –SiF$_3$ is considered as well. For comparison, the complexes of furanTF$_3$ and NH$_3$ are also studied. To probe the influence of O/N protonation on the strength of tetrel bonding, we perform analyses via molecular electrostatic potentials, atoms in molecules (AIM), natural bond orbital (NBO), and energy decomposition.

<Scheme 1>

2. Theoretical methods

The structures of complexes and monomers were first optimized at the MP2/aug-cc-pVDZ level. Then frequency calculations were performed at the same level to affirm that these structures correspond to minima on the potential surfaces. To obtain more reliable results, these structures were again optimized at the MP2/aug-cc-pVTZ level. Interaction energies E_{int} were computed as the difference between the energy sum of the monomers and the energy of the complex, $E_{int}(AB) = \{E(A) + E(B)\} - E(AB)$, where the geometries of monomers were taken as those within the complex. Binding energies E_b refer to the monomers in their isolated optimized geometries as reference point. These two quantities thus differ by the deformation energy DE required to change the monomer geometries from optimized structures to those adopted within the complex. The counterpoise procedure of Boys and Bernardi[70] was used to evaluate the basis set superposition error (BSSE) correction for these energies. In spite of a recent work that suggested[71] that BSSE corrected energies deviate more from the basis set limit values than uncorrected ones in the Be_2 system, a raft of prior work has demonstrated the necessity of this correction which is now included in studies of interactions as a matter of course.[72-79] All calculations were carried out using the Gaussian 09 program.[80]

Molecular electrostatic potentials (MEPs) on the 0.001 au contour of electron density were calculated at the HF/aug-cc-pVTZ level using the wave function analysis−surface analysis suite (WFA-SAS) program.[81] Natural bond orbital (NBO) analysis[82] was implemented at the WB97XD/aug-cc-pVDZ level[83] via NBO 3.0 in Gaussian 09 to analyze orbital interaction and charge transfer. Topological properties were derived from the theory of atoms in molecules (AIM) at the MP2/aug-cc-pVTZ level with the AIM2000 software.[84] To gain further insight into the nature of the investigated intermolecular interactions, we performed energy decomposition analysis (EDA) at the MP2/aug-cc-pVTZ level using the GAMESS program.[85]

3. Results and discussion

3.1 Tetrel bonds in the neutral complexes

<Figure 1>

Fig. 1 presents the MEP map of *p*-PySiF$_3$. Four red regions (σ–holes) are found on the tetrahedral surface of the Si atom, located opposite the C–Si and Si–F bonds. For easy comparison, the MEP on the σ–hole opposite the C–Si bond is labelled as $V_{max,1}$, and those opposite the Si–F bonds as $V_{max,2}$, $V_{max,3}$, and $V_{max,4}$, respectively. Their specific representation is seen in Fig. 1. Similar features are also found in other molecules furanTF$_3$ and PyTX$_3$ (X = F and Cl) with the exception of *p*-PyCF$_3$. The values of the most positive MEPs on these four σ–holes in all molecules furanTF$_3$ and PyTX$_3$ are listed in Table S1. Obviously, the σ–hole opposite the C–T bond (T = tetrel atom) is not the largest among these σ–holes. Even so, we only focus on the σ–hole at the C–T end to stress the tetrel bonding between furanTF$_3$/PyTX$_3$ and NH$_3$. Some trends are observed for the C-T σ–hole. Firstly, this σ–hole is larger for the heavier T atom. This is attributed to the smaller electronegativity and larger polarizability of the heavier T atom. Secondly, the σ–hole in α-furanTF$_3$ is greater than that in β-furanTF$_3$ and it becomes larger in the order *o*-PySiF$_3$<*m*-PySiF$_3$<*p*-PySiF$_3$. Obviously, the relative position of –TF$_3$ with respect to the O/N atom has an effect on the σ–hole. Thirdly, the σ–hole is smaller in *p*-PySiCl$_3$ than that in *p*-PySiF$_3$ due to the lesser electronegativity of Cl. In addition, $V_{max,4}$ is much larger than $V_{max,2}$ and $V_{max,3}$ in α/β-furanTF$_3$ (T = Si and Ge) due to the stronger electron-withdrawing ability of the oxygen atom in furan.

<Figure 2>

As expected, the C–T σ–hole in the molecules furanTF$_3$ and PyTX$_3$ can form a tetrel bond with NH$_3$. The optimized structures of neutral complexes furanTF$_3$···NH$_3$ and PyTX$_3$···NH$_3$ (T = C, Si, Ge; X = F, Cl) are displayed in Fig. 2. However, tetrel-bonded complexes are not obtained for α/β-furanCF$_3$ and *p*-PyCF$_3$, which revert to a F···H bonded complex during the optimization. The corresponding binding energies are listed in Table 1. It is found that the binding energy has a consistent correlation with the positive MEP on the C–T σ–hole in the molecules furanTF$_3$ and PyTX$_3$ (see their linear relationship in Fig. S1). Specifically, the binding energy grows in the order **11/12** < **8/9**, **5** < **6** < **2**, **2** < **3**, and **4** < **2**. This suggests the importance of electrostatic interaction in tetrel bonding. Also the strength of tetrel bonding is associated with the nature of the T atom, substitution position of the –SiF$_3$ group, and the electronegativity of the X atom. Clearly, the binding energy in these complexes is very large, up to 29.31 kcal/mol in **3**. The strong tetrel bonding leads to a prominent deformation of –SiX$_3$. For example, the angle ∠C–Si–F is ~110° in the monomer PySiF$_3$ but is reduced to ~98° in the neutral complex PySiF$_3$···NH$_3$. Thus, the deformation energy amounts to more than 70% of the binding energy for the tetrel bond. In addition, the binding energy is very small in **1**, **7**, and **10**, where a weak F···H interaction is the primary attractive force.

<Table 1>

If NH$_3$ attacks *p*-PySiF$_3$ along the Si–F bond, as opposed to C–Si, can a corresponding tetrel-bonded complex be obtained? Indeed it can, with the corresponding structure shown in Fig. S2. However, only one structure along the Si–F end is obtained although there are three such Si–F σ–holes. Furthermore, the structure in Fig. S2 exhibits a longer binding distance and smaller binding energy than that in Fig. 2. Accordingly, the σ–hole along the Si–F end forms a weaker tetrel bond with NH$_3$ than that at the C–Si end. Surprisingly, this is not in agreement with the magnitudes of the positive MEP on the Si–F and C–Si ends (Table S1). Clearly, –SiF$_3$ suffers a larger deformation in Fig. 2 than that in Fig. S2. Thus the deformation energy (more than 20 kcal/mol) is important in determining the strength of this tetrel bond. When –TF$_3$ is replaced by –TH$_3$ (Fig. S3), the binding energy is 3.02 kcal/mol and 2.44 kcal/mol in the complexes *p*-PySiH$_3$···NH$_3$ and *p*-PyGeH$_3$···NH$_3$, respectively, with binding distances of 3.032 Å.

Clearly, the Si/Ge···N interaction is much weaker in *p*-PySiH$_3$···NH$_3$ and *p*-PyGeH$_3$···NH$_3$ than that in the –TF$_3$ analogues. This is in line with the weaker electron-withdrawing ability of hydrogen atoms. Moreover, the tetrel bond is stronger in *p*-PySiH$_3$···NH$_3$ than that in *p*-PyGeH$_3$···NH$_3$, opposite to that in *p*-PySiF$_3$···NH$_3$ and *p*-PyGeF$_3$···NH$_3$.

The binding distances and change of C–T bond length are respectively represented with standard and italic numbers in Fig. 2. The Si···N distance in the complexes furanSiF$_3$···NH$_3$ and PySiX$_3$···NH$_3$ is within the range of 2.055~2.120 Å, which is much shorter than the sum of van der Waals radii of both atoms (~3.7 Å).[86] This is in line with the strong tetrel bond in these complexes. In all, the shorter Si···N distance corresponds to a stronger tetrel bond with greater binding energy. Due to the larger atomic radius of the Ge atom, the Ge···N distance in **3** is longer than R(Si···N) in **2**, although the former complex has the larger binding energy. A similar result is also found between **8** and **9**. However, the Ge···N distance in **12** is smaller than the Si···N value in **11** due to the larger difference of binding energy in both complexes. The F···H distance in **1** is shorter than that in **7**, but the binding energy in the former complex is smaller than that in the latter one. The main reason for this trend is the presence of two F···H interactions in **7** but only one such F···H interaction in **1**. The larger separation between the O and the F atoms in **10** than in **7** is responsible for the shorter F···H distance and the larger binding energy in the former. The C–T bond is lengthened whether in the tetrel-bonded complexes or in the hydrogen-bonded complexes with the exception of **10**, although its elongation in the former complex is more prominent than in the latter. The T–X bond is also elongated in the tetrel-bonded complexes and suffers only a small change in the hydrogen-bonded complexes (Table S2).

Fig. S4 shows the AIM bonding diagrams of the neutral complexes furanTF$_3$···NH$_3$ and PyTX$_3$···NH$_3$. The tetrel bond is characterized by a T···N BCP (a small red point) and the hydrogen bond by a F···H BCP. Additionally, a N···H BCP and a Cl/F···H BCP are also found in **1**/**10** and **4**/**9**, respectively. The T···N BCP has a positive Laplacian and a negative energy density, indicating the tetrel bond exhibits partially covalent nature.[87] The electron density at the Si···N BCP has an exponential relationship with the Si···N distance in the tetrel bond (Fig. S5), like that in hydrogen bonds.[88] The electron density at the F···H BCP is much smaller and the energy density at the F···H BCP is positive; thus the F···H interaction in **1**, **7**, and **10** is very weak.

There are two main orbital interactions Lp$_N$→BD*$_{C–T}$ and Lp$_N$→BD*$_{T–X}$ in the tetrel bonded complexes, and their second-order NBO perturbation energies are represented by E^2(1) and E^2(2), respectively, in Table 1. (E^2(2) is the sum of three Lp$_N$→BD*$_{T–X}$ orbital interactions). The Lp$_N$→BD*$_{C–T}$ orbital interaction is responsible for the elongation of the C–T bond in the tetrel bond and the elongation of the T–X bond is caused by the Lp$_N$→BD*$_{T–X}$ orbital interaction. The Lp$_N$→BD*$_{T–X}$ orbital interaction is stronger than Lp$_N$→BD*$_{C–T}$. Generally, both orbital interactions are correlated with the binding energy of tetrel bonding in the complexes of furanTF$_3$ and PyTF$_3$ (T = Si and Ge) (Fig. S6). However, both Lp$_N$→BD*$_{C–T}$ and Lp$_N$→BD*$_{T–X}$ in **4** are stronger than those in **2**, showing a reverse change with the binding energy of tetrel bonding. This suggests that the contribution of orbital interaction to the stabilization of tetrel bonding is perhaps less influential than that of electrostatic interaction. Only one orbital interaction, Lp$_F$→BD*$_{N–H}$, is found in the hydrogen bond, and this orbital interaction is weaker in **7** than in **1**, showing a consistent change with the F···H distance. Similarly, the Lp$_F$→BD*$_{N–H}$ interaction is stronger in **10** than in **1**, consistent with the stronger hydrogen bond in the former.

The formation of each complex results in a charge transfer from the Lewis base to the Lewis acid (Table 1). The strong tetrel bond is accompanied by a large charge transfer; in contrast, a very small charge transfer occurs in the weak hydrogen bond. The charge transfer is correlated with the binding energy in the tetrel-bonded complexes with the exception of **4**.

In Table S3, the interaction energy is decomposed into five components: electrostatic (E^{ele}), exchange (E^{ex}), repulsion (E^{rep}), polarization (E^{pol}), and dispersion (E^{disp}). For the tetrel bond, the electrostatic energy is more negative than the polarization energy, and the dispersion energy is the smallest. Moreover, the polarization energy is less than half of the electrostatic energy in all complexes except **4**. Consequently, the tetrel bond is dominated by the electrostatic interaction. The relatively large polarization energy suggests that the orbitals undergo a significant change. Interestingly, the dispersion energy is larger in **4** than in the other complexes, consistent with the larger Cl atom as compared to F. For the weak hydrogen bond, the dispersion energy is largest and the polarization energy is smallest, the electrostatic energy is comparable with the dispersion energy in **7**.

3.2 Tetrel bonds in protonated complexes

The optimized structures of the protonated complexes H$^+$-furanTF$_3$···NH$_3$ and H$^+$-PyTX$_3$···NH$_3$ are presented in Fig. 2. When the O/N atom of furan/pyridine is protonated, the tetrel-bonded complexes of H$^+$-**1**, H$^+$-**7**, and H$^+$-**10** are obtained due to the enhancement of the σ–hole at the C–C end, which amounts to 85.81, 100.38, and 88.86 kcal/mol in H$^+$-*p*-PyCF$_3$, H$^+$-α-furanCF$_3$, and H$^+$-β-furanCF$_3$ (Table S4), respectively. Interestingly, when the proton in these complexes is removed, the tetrel-bonded structures are again changed to hydrogen-bonded ones in the optimization. This shows that the interaction mode between α/β-furanCF$_3$/*p*-PyCF$_3$ and NH$_3$ can be modulated through protonation. Protonation affects not only the magnitude of the σ–hole on the C atom but the sign of MEP on the F atom, varying from negative in the neutral molecule to positive in the protonated molecule.

<Table 2>

Compared with the neutral complexes, the Si/Ge···N binding distance is much shorter and the binding energy larger in the protonated analogues (Table 2). This shows that the Si/Ge···N tetrel bond is enhanced by the protonation on the O/N atom of furanTF$_3$/PyTX$_3$. A similar effect was also found in pnicogen bonds.[89] Moreover, the shortening of the Si/Ge···N binding distance is prominent (-0.049 ~ -0.137 Å) and the increase of binding energy is very large, from 14.15 kcal/mol in H$^+$-**4** to 30.09 kcal/mol in H$^+$-**8**. This indicates that the protonation is a very effective method for strengthening a tetrel bond. The influence of protonation on the strength of tetrel bonding is larger than that on the strength of pnicogen bonding. For the latter the binding energy is increased by 2.80 ~ 8.28 kcal/mol in PyZX$_2$ (Z = P, As; X = H, F).[89] Generally, the weaker the tetrel bond, the smaller both the shortening of Si···N binding distance and the increase of binding energy. There is an

exception in H^+-**4**, H^+-**8,** and H^+-**9**. The increase of binding energy in H^+-**8**/**9** is larger than that in H^+-**11**/**12**; in contrast, the increase of binding energy in H^+-**4** is smaller than that in H^+-**2**. Interestingly, the tetrel bond is weaker in the order H^+-**5**>H^+-**6**>H^+-**2** (longer Si···N distance and smaller binding energy), opposite to that in the neutral complexes. This suggests that protonation can change the order of tetrel bonding strength. In addition, the contribution of deformation energy to the binding energy of tetrel bond is smaller in the protonated complex than that in the neutral analogue.

The enhancement of tetrel bonding is consistent with the increase of electron density at the T···N BCP in the protonated complexes relative to their neutral analogues. Protonation also leads to an increase of acidity of the C–H bond, allowing it to bind with an F atom in H^+-**5** through a H···F path. The C···N tetrel bonding in H^+-**1**, H^+-**7**, and H^+-**10** is characterized by three F···N BCPs but no C···N BCP. This supports the conclusion that bond critical points are sometimes imperfect as indicators of a stabilizing interaction.[90] Even so, the electron density at the F···N BCP in H^+-**7**, and H^+-**10** is greater than that in H^+-**1**, showing a consistent change with the binding energy. The C···N tetrel bonding is a weak and closed-shell interaction, with positive Laplacian and energy density, while the Si/Ge···N tetrel bond is a strong interaction with the nature of a partially covalent bond.

<Figure 3>

One can see in Table S4 that the σ–hole on the C–T end is more intense in the protonated molecules. Thus it can form a stronger tetrel bond in the protonated complexes. Fig. 3 plots the relationship between the change of the most positive MEP on the σ–hole of the C–T end and the change of tetrel bonding energy in the protonated molecules. Obviously, the greater the increase of the σ–hole on the C–T end, the larger the increase of the binding energy. The increase of the σ–hole on the C–Si end increases in the order H^+-*p*-$PySiF_3$<H^+-*m*-$PySiF_3$<H^+-*o*-$PySiF_3$. That is, the effect of the protonation on the magnitude of the σ–hole on the C–Si end is related to the substitution position of $–SiF_3$. Specifically, the protonation greatly enlarges the σ–hole of the ortho-substituted–SiF_3 group. Similarly, the increase of the σ–hole on the C–T end in H^+-α-$furanTF_3$ is also larger than that in H^+-β-$furanTF_3$ (T = Si and Ge). The positive MEP on the σ–hole on the C–C end is large enough in H^+-α/β-$furanCF_3$ and H^+-*p*-$PyCF_3$, but the tetrel bonding energy in the corresponding complex is very small with respect to the Si and Ge complexes. This suggests that other contributions including polarization are also important in determining the energy of tetrel bonding (see the energy decomposition analysis below).

<Table 3>

After the protonation, two orbital interactions $Lp_N \rightarrow BD^*_{C–T}$ and $Lp_N \rightarrow BD^*_{T–X}$ become stronger (Table 3). Consequently, the elongation of the C–T bond is greater in the protonated complexes. The corresponding charge transfer is also increased, and its increase displays a good linear relationship with the change of binding energy (Fig. 4). This shows that the increase of charge transfer is at least partly responsible for the enhancement of tetrel bonding. Obviously, a great deal of charge transfer occurs in the strong Si/Ge···N interaction, much reduced in the weak C···N interaction (0.002e). The charge transfer in the strong Si/Ge···N interaction amounts to more than 0.2e, and the largest one takes place in H^+-**9**. The small charge transfer in the weak C···N interaction is consistent with weak orbital interaction.

<Figure 4>

As was the case in the unprotonated complexes, the electrostatic energy is still dominant (Table 4) after protonation. However, the increased percentage of polarization energy is larger than that of electrostatic energy in the Si/Ge···N interaction. This indicates that protonation has a greater effect on the polarization energy, consistent with the greater polarizability of the Si/Ge atom. In H^+-**1**, H^+-**7**, and H^+-**10**, the polarization energy is the smallest, corresponding to the weak polarizability of the C atom. The small polarization energy is partly responsible for the lower binding energy in H^+-**1**, H^+-**7**, and H^+-**10**, although the positive MEP on the C atom is relatively large. The dispersion energy is positive in most complexes, as was also reported for Li^+F^- and Na^+F^-, where the authors ascribed it to the differences in the intra- and interionic correlation energy on going from noninteracting to interacting ions, sensitive to basis set and distance.[91] Moreover, the dispersion energy becomes less negative in all protonated complexes. Actually, due to its small magnitude, dispersion makes only a small contribution to the protonation effect even though its changed percentage is large. As expected, the sum of the components obtained by the energy decomposition is almost equal to the full binding energy with the supermolecular method in Table 2.

<Table 4>

3.3 Competition between tetrel bond and hydrogen bond in the protonated complexes

As expected, the proton in the protonated system can engage in a hydrogen bond with NH_3. Thus we are interested in the competition between tetrel bonding and hydrogen bonding in the protonated complexes. Fig. 5 shows the optimized structures of the hydrogen-bonded complexes of $H_3N\cdots H^+$-*p*-$PyTX_3$ (T = C, Si, Ge; X = F, Cl) and $H_3N\cdots H^+$-*o*/*m*-$PySiF_3$. The hydrogen-bonded complexes of $H_3N\cdots H^+$-α/β-$furanTF_3$ are not studied since they transform to α/β-$furanTF_3$ and NH_4^+ in the optimization. The binding energy of hydrogen bonding is 24.45 kcal/mol in **13**, which is much larger than that of tetrel bonding in H^+-**1**. Thus the electron donor prefers to form a hydrogen bond with the proton of H^+-*p*-$PyCF_3$. However, the binding energy of hydrogen bonding in **14**-**18** is less than half that of tetrel bonding in H^+-(**2**-**6**). Consequently, the electron donor prefers binding with H^+-*p*-$PyTX_3$ (T = Si, Ge; X = F, Cl) and H^+-*o*/*m*-$PySiF_3$ through a tetrel bond rather than a hydrogen bond.

<Figure 5>

The hydrogen bond energy grow in the sequence **14**<**13**<**15**. The MEP on the proton in H^+-*p*-$PyTF_3$ (T = C, Si, Ge) is 160.57, 158.30 and 161.11 kcal/mol, respectively. This supports the role of electrostatic interaction in the formation of hydrogen bonding. Similarly, the hydrogen bonding in **14** is stronger than that in **16**. The hydrogen bond energy in **14** is smaller than that in **17** but is almost equal to that in **18**. This shows that the substitution position of $–SiF_3$ has an effect on the strength of hydrogen bonding. The binding energy of hydrogen bonding in **14**-**18** is larger than that in $H_3N\cdots H^+$-*p*-PyH (22.74 kcal/mol). This indicates that the $–TX_3$ group in the proton

donor plays an electron-withdrawing role in the formation of hydrogen bonding. Moreover, the electron-withdrawing role of this group grows in the $–SiCl_3$<$–SiF_3$<$–CF_3$<$–GeF_3$ sequence, showing an irregular dependence on the T atom. The electron-withdrawing ability of $–SiF_3$ is also correlated with the separation distance between the proton and this group. The electron-withdrawing role of the $–TX_3$ group is confirmed by a decrease of the positive charge on this group in the hydrogen-bonded complexes (Table S5).

The N···H distance is in the range of 1.63-1.67 Å, which is much shorter than the sum of van der Waals radii of both atoms (~2.8 Å). Clearly, the N···H distance has a consistent change with the binding energy of hydrogen bonding. That is, shorter binding distance corresponds to larger binding energy. Interestingly, the N···H binding energy is more negative than 22 kcal/mol, although it is smaller than that of an ion-pair hydrogen bond in AsO_2F:CNH:CNLi (28.7 kcal/mol).[92] Thus the shorter binding distance and larger binding energy indicate that the N···H interaction is a proton-shared hydrogen bond.

Expectedly, the formation of a hydrogen bond leads to an elongation of the N–H bond which correlates with the binding energy. It is found that the elongation of N–H bond (0.062-0.071 Å) is fairly large due to the strong hydrogen bond. The strong hydrogen bond is also accompanied by a large degree of charge transfer (0.122-0.133e in Table S5). Fig. S6 shows the good linear relationship between the charge transfer and the binding energy in the hydrogen-bonded complexes **13**-**16** and **18** with a correlation coefficient of 0.983. This shows that charge transfer is an important component in stabilizing the hydrogen-bonded complexes. NBO analysis indicates that there are two weak N–H···F interactions in **17**, with a reverse charge transfer with the tetrel bond: **17** has the smaller charge transfer but the larger binding energy than **15**.

The strong hydrogen bond is also characterized by the negative energy density at the N···H BCP (Table S6), indicating that the hydrogen bond is a partially covalent interaction.[87] Even so, the N···H hydrogen bond is dominated by electrostatic energy although there are substantial contributions from polarization (Table S7).

4. Conclusions

The complexes of furanTF_3/$PyTX_3$ (T = C, Si, Ge; X = F, Cl) and NH_3 have been studied from a theoretical perspective. Based on the analyses of the structures, energies, NBO, AIM, and energy decomposition of these complexes, the following conclusions have been reached.

Protonation can modulate the interaction type, varying from a F···H hydrogen bond in the neutral complexes of α/β-furanCF_3 and *p*-$PyCF_3$ to a tetrel bond in the protonated counterparts.

Protonation greatly strengthens Si/Ge···N tetrel bonding, and its binding energy is increased by 14.15 - 30.09 kcal/mol, depending on the nature of the T and X atoms as well as the relative position of $–SiF_3$ with respect to the O/N atom.

Protonation can affect the relative order of tetrel bonding strength. The tetrel bond becomes stronger in the *o*-$PySiF_3$···NH_3<*m*-$PySiF_3$···NH_3<*p*-$PySiF_3$···NH_3 order but weakens in the same order for the protonated analogues.

Protonation has an increasing effect on the contributions from electrostatic and polarization energies. For the Si/Ge···N tetrel bonding, the increased percentage of polarization energy is about twice as much as that of electrostatic energy.

A competition is found between the tetrel and hydrogen bonds in the protonated complexes of NH_3 with H^+-*p*-$PyTX_3$ (T = C, Si, Ge; X = F, Cl) as well as H_3N···H^+-*o*/*m*-$PySiF_3$. The hydrogen-bonded complex is more stable than the tetrel bonded complex for the complexes of H^+-*p*-$PyCF_3$, while the reverse is found in the other complexes. These results may be of significance in biochemical processes involving protonation.

Acknowledgements

This work was supported by the National Natural Science Foundation of China (21573188) and the Graduate Innovation Foundation of Yantai University (YDZD1608).

References

1. S. Scheiner, *Noncovalent Forces*, Springer, 2015.
2. A. Bauzá, T. J. Mooibroek and A. Frontera, *Angew. Chem. Int. Ed.*, 2013, **52**, 12317–12321.
3. A. Bauzá, T. J. Mooibroek and A. Frontera, *Chem. Rec.*, 2016, **16**, 473–487.
4. A. Bauzá, T. J. Mooibroek and A. Frontera, *Chem. Commun.*, 2014, **50**, 12626–12629.
5. S. P. Thomas, M. S. Pavan and T. N. G. Row, *Chem. Commun.*, 2014, **50**, 49–51.
6. D. Mani and E. Arunan, *ChemPhysChem*, 2013, **14**, 754–763.
7. X. L. Dai, S. B. Choi, C. W. Braun, P. Vaidya, S. Kilina, A. Ugrinov, D. L. Schulz and P. Boudjouk, *Inorg. Chem.*, 2011, **50**, 4047–4053.
8. G. Mahmoudi, A. Bauzá and A. Frontera, *Dalton Trans.*, 2016, **45**, 4965–4969.
9. G. Mahmoudi, A. Bauzá, M. Amini, E. Molins, J. T. Mague and A. Frontera, *Dalton Trans.*, 2016, **45**, 10708–10716.
10. M. S. Gargari, V. Stilinović, A. Bauzá, A. Frontera, P. McArdle, D. V. Derveer, S. W. Ng and G. Mahmoudi, *Chem. Eur. J.*, 2015, **21**, 17951–17958.
11. S. A. Southern and D. L. Bryce, *J. Phys. Chem. A*, 2015, **119**, 11891–11899.
12. J. S. Murray, P. Lane and P. Politzer, *J. Mol. Model.*, 2009, **15**, 723–729.
13. S. Scheiner, *J. Phys. Chem. A*, 2015, **119**, 9189−9199.
14. L. M. Azofra, S. Scheiner, *J. Chem. Phys.*, 2015, **142**, 034307.
15. S. A. C. McDowell and J. A. Joseph, *Phys. Chem. Chem. Phys.*, 2014, **16**, 10854−10860.
16. D. Mani and E. Arunan, *J. Phys. Chem. A*, 2014, **118**, 10081−10089.
17. Q. Z. Li, H. Y. Zhuo, H. B. Li, Z. B. Liu, W. Z. Li and J. B. Cheng, *J. Phys. Chem. A*, 2014, **119**, 2217−2224.
18. Q. Z. Li, X. Guo, X. Yang, W. Z. Li, J. B. Cheng and H. B. Li, *Phys. Chem. Chem. Phys.*, 2014, **16**, 11617−11625.
19. M. D. Esrafili and F. Mohammadian-Sabet, *J. Mol. Model.*, 2015, **21**, 60.
20. V. de P. N. Nziko and S. Scheiner, *Phys. Chem. Chem. Phys.*, 2016, **18**, 3581–3590.
21. J. S. Murray, M. C. Concha and P. Politzer, *J. Mol. Model.*, 2011, **17**, 2151–2157.
22. X. L. Dai, K. J. Anderson, D. L. Schulz and P. Boudjouk, *Dalton Trans.*, 2010, **39**, 11188–11192.
23. A. M. G. Voronkov, E. A. Grebneva, O. M. Trofimova, N. F. Chernov, A. I. Albanov and N. N. Chipanina, *Doklady Chem.*, 2006, **409**, 139–141
24. J. Mikosch, S. Trippel, C. Eichhorn, R. Otto, U. Lourderaj, J. X. Zhang, W. L. Hase, M. Weidemüller and R. Wester, *Science*, 2008,

319, 183–186.
25. S. J. Grabowski, *Phys. Chem. Chem. Phys*., 2014, **16**, 1824–1834.
26. A. Bauzá, R. Ramis and A. Frontera, *Comput. Theor. Chem.,* 2014, **1038**, 67–70.
27. A. Robertazzi, J. A. Platts and P. Gámez, *ChemPhysChem*, 2014, **15**, 912–917.
28. K. J. Donald and M. Tawfik, *J. Phys. Chem. A*, 2013, **117**, 14176–14183.
29. A. Bundhun, P. Ramasami, J. S. Murray and P. Politzer, *J. Mol. Model*., 2013, **19**, 2739–2746.
30. M. X. Liu, Q. Z. Li, W. Z. Li, J. B. Cheng and Sean A. C. McDowell, *RSC Adv*., 2016, **6**, 19136–19143.
31. A. Bauzá and A. Frontera, *Crystals*, 2016, **6**, 26.
32. A. Bauzá, A. Frontera and T. J. Mooibroek, *Phys. Chem. Chem. Phys*., 2016, **18**, 1693–1698.
33. A. Bauzá, T. J. Mooibroek and A. Frontera, *Chem. Rec.*, 2016, **16**, 473–487.
34. A. Bauzá and A. Frontera, *ChemPhysChem*, 2015, **16**, 3108–3113.
35. R. S. Ruoff, T. Emilsson, A. I. Jaman, T. C. Germann and H. S. Gutowsky, *J. Chem. Phys*., 1992, **96**, 3441−3446.
36. K. Tamao, T. Hayashi and Y. Ito, *J. Organomet. Chem.*, 1996, **506**, 85−91.
37. R. D. Urban, G. Rouillé and M. Takami, *J. Mol. Struct*., 1997, **413-414**, 511−519.
38. N. W. Mitzel, A. J. Blake and D. W. H. Rankin, *J. Am. Chem. Soc.,* 1997, **119**, 4143−4148.
39. N. W**.** Mitzel and U. Losehand, *Angew. Chem. Int. Ed. Engl.,* 1997, **36**, 242807−2809.
40. K. B. Borisenko, R. O. Gould, C. A. Morrison, S. Parsons and D. W. H. Rankin, *J. Mol. Struct.*, 2000, **554**, 163–172.
41. I. Alkorta, I. Rozas and J. Elguero, *J. Phys. Chem. A,* 2001, **105**, 743–749.
42. K. Vojinovic, L. J. McLachlan, S. L. Hinchley, D.W. H. Rankin and N. W. Mitzel, *Chem. Eur. J.,* 2004, **10**, 3033–3042.
43. X. Guo, Y. W. Liu, Q. Z. Li, W. Z. Li and J. B. Cheng, *Chem. Phys. Lett*., 2015, **620**, 7–12.
44. M. X. Liu, Q. Z. Li, W. Z. Li and J. B. Cheng, *J. Mol. Graphics Model*., 2016, **65**, 35–42.
45. M. D. Esrafili, N. Mohammadirad and M. Solimannejad, *Chem. Phys. Lett*., 2015, **628**, 16–20.
46. S. Yourdkhani, T. Korona and N. L. Hadipour, *J. Comput. Chem*., 2015, **36**, 2412–2428.
47. M. Marín-Luna, I. Alkorta and J. Elguero, *J. Phys. Chem. A*, 2016, **120**, 648−656.
48. Q. J. Tang and Q. Z. Li, *Comput. Theor. Chem*., 2014, **1050**, 51–57.
49. M. Solimannejad, M. Orojloo and S. Amani, *J. Mol. Model*., 2015, **21**, 183.
50. Z. Rezaei, M. Solimannejad and M. D. Esrafili, *Comput. Theor. Chem*., 2015, **1074**, 101–106.
51. M. D. Esrafili, R. Nurazar and F. Mohammadian-Sabet, *Mol. Phys.*, 2015, **113**, 3703–3711.
52. M. D. Esrafili and F. Mohammadian-Sabet, *Mol. Phys*., 2016, **114**, 1528–1538.
53. M. D. Esrafili and F. Mohammadian-Sabet, *Mol. Phys*., 2016, **114**, 83–91.
54. M. Vatanparast, E. Parvini and A. Bahadori, *Mol. Phys.*, 2016, **114**, 1478–1484.
55. M. D. Esrafili, M. Vakili, M. Javaheri and H. R. Sobhi, *Mol. Phys.*, 2016, **114**, 1974–1982.
56. B. Chan, J. E. Del Bene, J. Elguero and L. Radom, *J. Phys. Chem. A*, 2005, **109**, 5509−5517.
57. M. C. Sicilia, A. Niño and C. Muñoz-Caro, *J. Phys. Chem. A*, 2005, **109**, 8341−8347.
58. S. Scheiner and T. Kar, *J. Phys. Chem. B*, 2002, **106**, 534−539.
59. M. Makowski, R. Sadowski, D. Augustin-Nowacka and L. Chmurzyñski, *J. Phys. Chem. A*, 2001, **105**, 6743−6749.
60. D. A. Nichols, J. C. Hargis, R. Sanishvili, P. Jaishankar, K. Defrees, E, W. Smith, K. K. Wang, F. Prati, A. R. Renslo, H. L. Woodcock and Y. Chen, *J. Am. Chem. Soc*., 2015, **137**, 8086−8095.
61. M. Chan-Huot, A. Dos, R. Zander, S. Sharif, P. M. Tolstoy, S. Compton, E. Fogle, M. D. Toney, I. Shenderovich, G. S. Denisov and H. H. Limbach, *J. Am. Chem. Soc*., 2013, **135**, 18160−18175.
62. V. A. Levina, O. A. Filippov, E. I. Gutsul, N. V. Belkova, L. M. Epstein, A. Lledos and E. S. Shubina, *J. Am. Chem. Soc*., 2010, **132**, 11234–11246.
63. J. E. Del Bene, *J. Phys. Chem*., 1983, **87**, 367–371.
64. O. Lehtonen, J. Hartikainen, K. Rissanen, O. Ikkala and L.O. Pietilä, *J. Chem. Phys*., 2002, **116**, 2417–2424.
65. M. C. R. Delgado, J. Orduna, M. M. Oliva, J. Casado and J. T. L. Navarrete, *J. Chem. Phys*., 2007, **127**, 164704.
66. A. M. Hamid, M. S. El-Shall, R. Hilal, S. Elroby and S. G. Aziz, *J. Chem. Phys.*, 2014, **141**, 054305.
67. N. W. Mitzel, A. J. Blake and D. W. H. Rankin, *J. Am. Chem. Soc*., 1997, **119**, 4143–4148.
68. D. L. Reger, R. F. Semeniuc and M. D. Smith, *Cryst. Growth Des.*, 2005, **5**, 1181–1190.
69. G. M. Espallargas, L. Brammer, D. R. Allan, C. R. Pulham, N. Robertson and J. E. Warren, *J. Am. Chem. Soc*., 2008, **130**, 9058–9071.
70. S. F. Boys and F. Bernardi, *Mol. Phys.*, 1970, **19**, 553−556.
71. Ł. M. Mentel and E. J. Baerends, *J. Chem. Theory Comput*., 2014, **10**, 252–267.
72. E. Miliordos and S. S. Xantheas, *J. Chem. Phys*., 2015, **142**, 094311.
73. A. Roztoczynska, A. Kaczmarek-Kedziera, R. W. Góra and W. Bartkowiak, *Chem. Phys. Lett.*, 2013, **571**, 28–33.
74. J. A. Plumley and J. J. Dannenberg, *J. Comput. Chem.*, 2011, **32**, 1519–1527.
75. A. Baranowska, B. Fernández and A. J. Sadlej, *Theor. Chem. Acc*., 2011, **128**, 555–561.
76. P. Salvador, S. Simon, M. Duran and J. J. Dannenberg, *J. Chem. Phys.*, 2000, **113**, 5666–5674.
77. S. S. Xantheas, *J. Chem. Phys*., 1996, **104**, 8821–8824.
78. M. Gutowski and G. Chalasinski, *J. Chem. Phys*., 1993, **98**, 5540–5554.
79. M. M. Szczesniak and S. Scheiner, *J. Chem. Phys.*, 1986, **84**, 6328–6335.
80. M. J. Frisch, G. W. Trucks, H. B. Schlegel, G. E. Scuseria, M. A. Robb, J. R. Cheeseman, G. Scalmani, V. Barone, B. Mennucci, G. A. Petersson, H. Nakatsuji, M. Caricato, X. Li, H. P. Hratchian, A. F. Izmaylov, J. Bloino, G. Zheng, J. L. Sonnenberg, M. Hada, M. Ehara, K. Toyota, R. Fukuda, J. Hasegawa, M. Ishida, T. Nakajima, Y. Honda, O. Kitao, H. Nakai, T. Vreven, J. J. A. Montgomery, J. E. Peralta, F. Ogliaro, M. Bearpark, J. J. Heyd, E. Brothers, K. N. Kudin, V. N. Staroverov, R. Kobayashi, J. Normand, K. Raghavachari, A. Rendell, J. C. Burant, S. S. Iyengar, J. Tomasi, M. Cossi, N. Rega, J. M. Millam, M. Klene, J. E. Knox, J. B. Cross, V. Bakken, C. Adamo, J. Jaramillo, R. Gomperts, R. E. Stratmann, O. A. Yazyev, J. Austin, R. Cammi, C. Pomelli, J. W. Ochterski, R. L. Martin, K. Morokuma, V. G. Zakrzewski, G. A. Voth, P. Salvador, J. J. Dannenberg, S. A. Dapprich, D. Daniels, O. Farkas, J. B. Foresman, J. V. Ortiz, J. Cioslowski and D. J. Fox, Gaussian 09, Revision A.02, Gaussian, Inc., Wallingford, CT2009.
81. F. A. Bulat, A. Toro-Labbe, T. Brinck, J. S. Murray and P. Politzer, *J.*

Mol. Model., 2010, **16**, 1679−1691.
82. A. E. Reed, L. A. Curtiss and F. A. Weinhold, *Chem. Rev.*, 1988, **88**, 899–926.
83. Q. C. Wei, Q. Z. Li, J. B. Cheng, W. Z. Li and H. B. Li, *RSC Adv.*, 2016, **6**, 79245–79253.
84. F. Biegler-Konig, *AIM2000*, University of Applied Sciences, Bielefeld, Germany, 2000.
85. M. W. Schmidt, K. K. Baldridge, J. A. Boatz, S. T. Elbert, M. S. Gordon, J. H. Jensen, S. Koseki, N. Matsunaga, K. A. Nguyen, S. J. Su, T. L. Windus, M. Dupuis and J. A. Montgomery, *J. Comput. Chem*., 1993, **14**, 1347–1363.
86. A. Bondi, *J. Phys. Chem*., 1964, **68**, 441–445.
87. W. D. Arnold and E. Oldfield, *J. Am. Chem. Soc*., 2000, **122**, 12835–12841.
88. I. Alkorta, K. Zborowski, J. Elguero and M. Solimannejad, *J. Phys. Chem. A*, 2006, **110**, 10279–10286.
89. Y. X. Wei, Q. Z. Li, W. Z. Li, J. B. Cheng and S. A. C. McDowell, *Phys. Chem. Chem. Phys.*, 2016, **18**, 11348–11356.
90. J. Poater, M. Solá and F. M. Bickelhaupt, *Chem. Eur. J*., 2006, **12**, 2902–2905.
91. P. F. Su and H. Li, *J. Chem. Phys.*, 2009, **131**, 014102.
92. H. Y. Zhuo, Q. Z. Li, W. Z. Li and J. B. Cheng, *J. Chem. Phys.*, 2014, **141**, 244305.

Journal Name

ARTICLE

Table 1. Binding and interaction energy corrected with BSSE and deformation energy DE, (kcal/mol), charge transfer (CT, e) and second-order perturbation energies (E^2, kcal/mol) in the neutral complexes as well as the most positive MEP ($V_{max,1}$, kcal/mol) on the T atom at the C–T end of the neutral molecule.

	E_b	BSSE	DE	E_{int}	CT	$E^2(1)$	$E^2(2)$	$V_{max,1}$
p-PyCF_3···NH_3(**1**)	1.44	0.63	0.02	0.83	0.000	1.13	---	10.58
p-PySiF_3···NH_3(**2**)	5.95	2.11	22.49	26.33	0.167	18.73	76.25	41.56
p-PyGeF_3···NH_3(**3**)	12.65	3.83	20.49	29.31	0.192	14.18	94.42	41.57
p-Py$SiCl_3$···NH_3(**4**)	4.46	2.59	23.37	25.24	0.216	23.04	90.52	22.17
o-PySiF_3···NH_3(**5**)	4.75	2.09	21.90	24.56	0.161	18.14	73.96	34.86
m-PySiF_3···NH_3(**6**)	5.67	2.11	22.47	26.03	0.166	18.49	76.26	39.43
α-furanCF_3···NH_3(**7**)	1.45	0.47	0.02	1.00	0.002	0.61	---	7.38
α-furanSiF_3···NH_3(**8**)	6.00	2.14	22.34	26.20	0.165	18.45	75.96	37.96
α-furanGeF_3···NH_3(**9**)	12.54	3.89	20.26	28.91	0.190	14.71	92.48	38.96
β-furanCF_3···NH_3(**10**)	1.69	0.61	0.03	1.11	0.003	1.08	---	5.91
β-furanSiF_3···NH_3(**11**)	4.19	2.09	21.74	23.84	0.160	17.09	73.39	36.21
β-furanGeF_3···NH_3(**12**)	11.13	3.77	20.38	27.73	0.188	13.86	92.49	36.61

Note: $\Delta E_{corr} = \Delta E$ – BSSE + DE. CT is defined as the sum of NBO atomic charges on NH_3. $E^2(1)$ and $E^2(2)$ in **2-6, 8**, **9**, **11**, and **12** respectively correspond to the orbital interactions of $Lp_N \rightarrow BD^*_{C-T}$ and $Lp_N \rightarrow BD^*_{T-X}$, where Lp_N is the lone pair orbital on the N atom of NH_3, BD^*_{C-T} and BD^*_{T-X} respectively denotes the C–T and T–X anti-bonding orbitals in furanTF_3 or PyTX_3 (T=Si, Ge; X = F and Cl). $E^2(1)$ corresponds to the $Lp_F \rightarrow BD^*_{N-H}$ orbital interaction in **1**, **7**, and **10**.

Table 2. Dissociation energy (ΔE_{corr}, kcal/mol) corrected with BSSE and DE in the protonated complexes as well as the changes in the dissociation energy ($\Delta\Delta E$, kcal/mol), binding distance (ΔR, Å) and electron density (Δρ, au) at the Si/Ge···N BCP in the protonated complexes relative to the neutral counterparts

	ΔE	BSSE	DE	ΔE_{corr}	$\Delta\Delta E$	ΔR	Δρ
H^+-**1**	4.16	0.38	0.11	3.89	---	---	---
H^+-**2**	25.54	2.21	24.97	48.30	21.97	-0.110	0.018
H^+-**3**	31.79	4.08	20.38	48.09	18.78	-0.070	0.015
H^+-**4**	19.60	2.52	22.31	39.39	14.15	-0.049	0.009
H^+-**5**	30.05	2.22	25.18	53.01	28.44	-0.137	0.015
H^+-**6**	26.24	2.23	25.00	49.02	22.99	-0.115	0.019
H^+-**7**	5.55	0.41	0.17	5.31	---	---	---
H^+-**8**	32.88	2.21	25.62	56.29	30.09	-0.133	0.023
H^+-**9**	39.68	4.31	21.51	56.88	27.96	-0.096	0.022
H^+-**10**	4.37	0.39	0.13	4.11	---	---	---
H^+-**11**	27.22	2.23	24.96	49.95	26.11	-0.137	0.022
H^+-**12**	33.51	4.08	20.29	49.72	21.99	-0.085	0.018

Note: The data of $\Delta\Delta E$, ΔR, and Δρ are not shown in H^+-**1**, H^+-**7**, and H^+-**10** since there is not a tetrel bond in the neutral counterparts.

Table 3. Charge transfer (CT, e) and second-order perturbation energies (E^2, kcal/mol) in the protonated complexes as well as their change (Δ) relative to the neutral analogues at the WB97XD/aug-cc-pVDZ level

	CT	ΔCT	$E^2(1)$	$E^2(2)$	$\Delta E^2(1)$	$\Delta E^2(2)$
H^+-**1**	0.002	---	0.34	0.15	---	---
H^+-**2**	0.215	0.048	28.70	92.25	9.97	16.00
H^+-**3**	0.235	0.043	21.25	107.26	7.07	12.84
H^+-**4**	0.244	0.028	32.17	93.03	9.13	2.51
H^+-**5**	0.222	0.061	30.53	91.13	12.39	17.17
H^+-**6**	0.215	0.049	28.63	93.41	10.14	17.15
H^+-**7**	0.002	---	0.37	0.29	---	---
H^+-**8**	0.228	0.063	31.58	96.40	13.13	20.44
H^+-**9**	0.253	0.063	22.28	115.31	7.57	22.83
H^+-**10**	0.002	---	0.33	0.18	---	---
H^+-**11**	0.218	0.057	29.63	92.73	12.54	19.34
H^+-**12**	0.237	0.049	22.34	107.41	8.48	14.92

Note: The data of $\Delta E^2(1)$ and $\Delta E^2(2)$ are not shown in H^+-**1**, H^+-**7**, and H^+-**10** since there is not a tetrel bond in the neutral counterparts.

Table 4. Electrostatic energy (E^{ele}), exchange energy (E^{ex}), repulsion energy (E^{rep}), polarization energy (E^{pol}), dispersion energy (E^{disp}), and binding energy (E^{int}) in the protonated systems. All are in kcal/mol

	E^{ele}	E^{ex}	E^{rep}	E^{pol}	E^{disp}	E^{int}
H^+-**1**	-5.19	-3.82	6.86	-0.55	-1.18	-3.89
H^+-**2**	-94.50(26%)	-88.88(8%)	189.05(12%)	-54.74(50%)	0.50(-137%)	-48.57
H^+-**3**	-101.56(18%)	-90.14(2%)	196.21(6%)	-53.29(35%)	2.24(1218%)	-46.55
H^+-**4**	-101.13(8%)	-132.11(-2%)	267.11(0%)	-66.68(17%)	-7.12(-17%)	-39.93
H^+-**5**	-97.83(34%)	-89.36(10%)	191.43(16%)	-58.27(67%)	0.73(-151%)	-53.30
H^+-**6**	-94.81(28%)	-89.15(9%)	189.68(13%)	-54.94(52%)	-0.07(-96%)	-49.29
H^+-**7**	-6.96	-4.69	8.54	-0.76	-1.44	-5.31
H^+-**8**	-99.89(33%)	-89.69(9%)	192.95(14%)	-60.54(66%)	0.57(-141%)	-56.59
H^+-**9**	-108.23(26%)	-91.63(4%)	202.11(9%)	-59.81(53%)	2.5(3471%)	-55.05
H^+-**10**	-5.52	-3.98	7.16	-0.58	-1.19	-4.10
H^+-**11**	-95.66(34%)	-88.98(11%)	189.76(16%)	-55.89(65%)	0.55(-134%)	-50.23
H^+-**12**	-102.71(22%)	-89.98(3%)	196.50(7%)	-54.28(42%)	2.37(-6025%)	-48.10

Note: Data in parentheses are the increased/decreased percentage of energy term in the protonated complexes relative to the neutral analogues. For systems of furanCF_3 and PyCF_3, the tetrel bonded structures are not obtained for the neutral complexes, thus the percentage is not given for these systems.

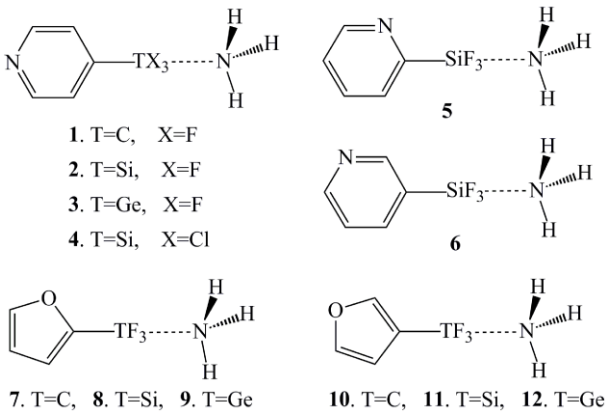

Scheme 1 Complexes **1-12**

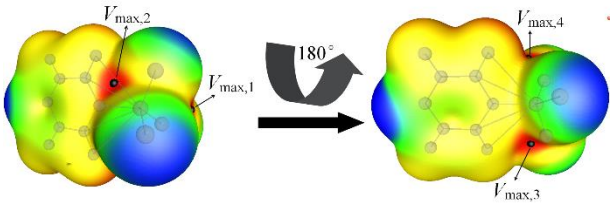

Fig. 1 MEP maps of *p*-$PySiF_3$. The black dot represents the most positive MEP on the Si atom (V_{max}, kcal/mol). Color ranges, in kcal/mol, are: Red, greater than 25.12; yellow, between 25.12 and 0; green, between 0 and -10.87; and blue, less than -10.87

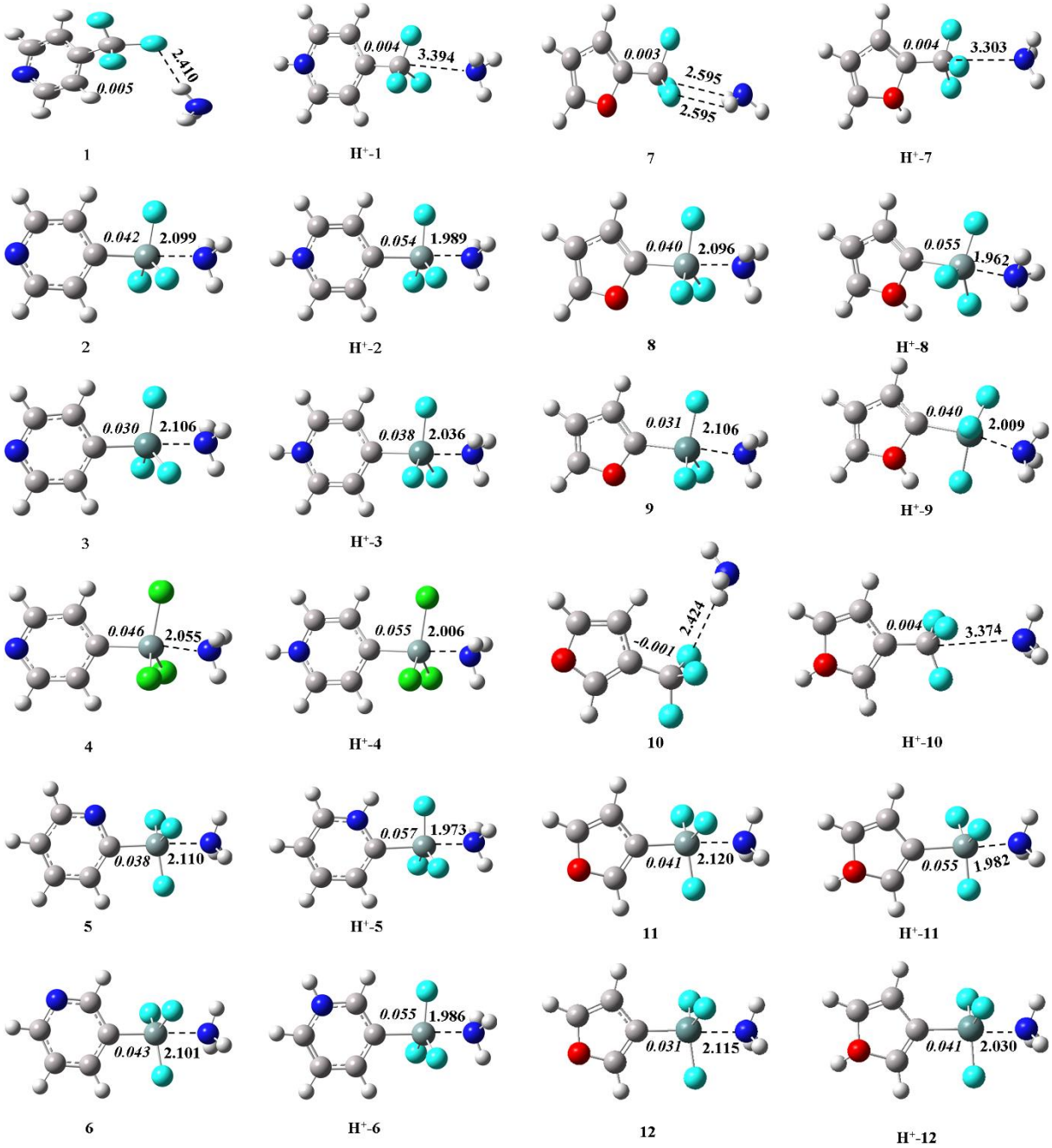

Fig. 2 Optimized structures of the neutral and protonated complexes. The binding distances (standard) and change of C–T bond length (italic) are in angstrom

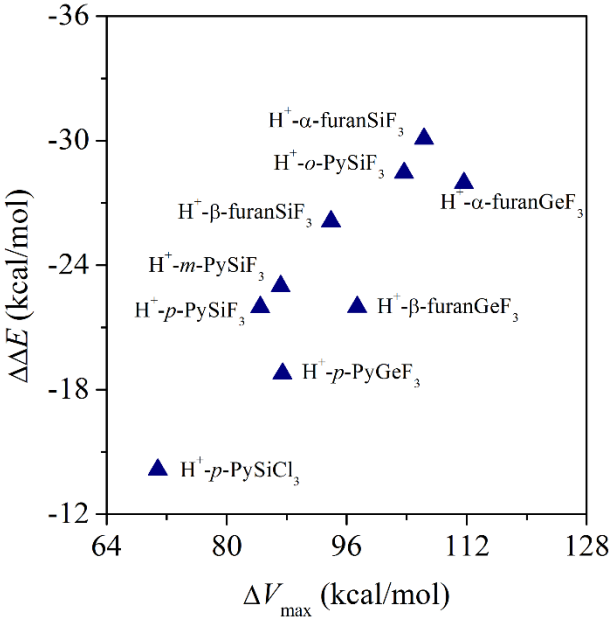

Fig. 3 Change of dissociation energy of tetrel bonding (ΔΔ*E*) in the protonated complexes of H^+-furanTF_3···NH_3 and H^+-PyTX_3···NH_3 (T = Si and Ge; X = F and Cl) relative to the neutral analogues versus change of the most positive MEP ($\Delta V_{max,1}$) on the T atom in the protonated molecules of furanTF_3/PyTX_3 relative to the neutral analogues

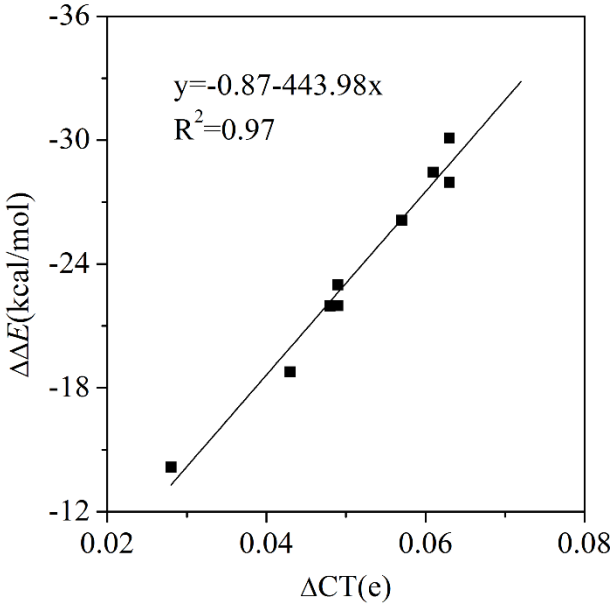

Fig. 4 Change of dissociation energy (ΔΔ*E*) versus change of charge transfer (ΔCT) of tetrel bonding in the protonated complexes of H^+-furanSiF_3···NH_3 and H^+-PyTX_3···NH_3 (T = Si and Ge; X = F and Cl) relative to the neutral analogues

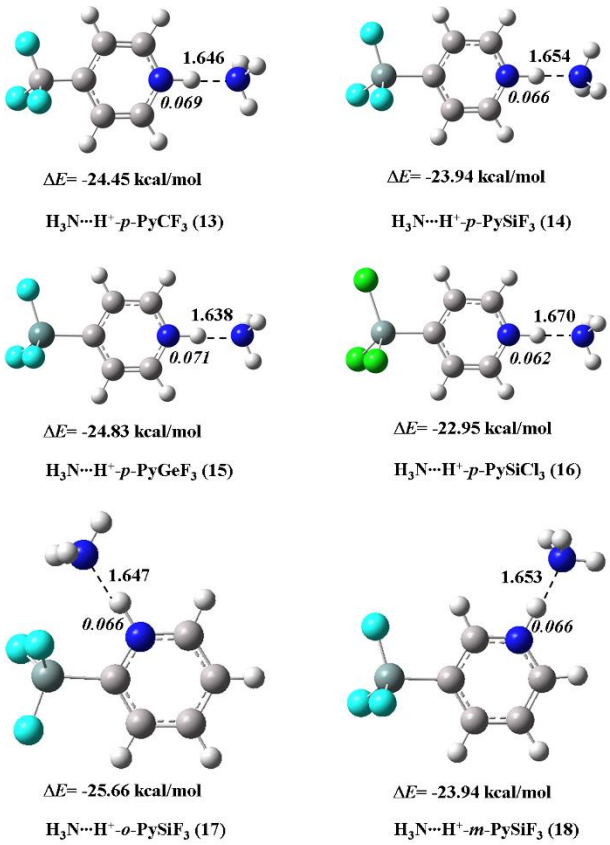

Fig. 5 Optimized structures of the hydrogen-bonded complexes. The binding distances (standard) and change of N–H bond length (italic) are in angstrom

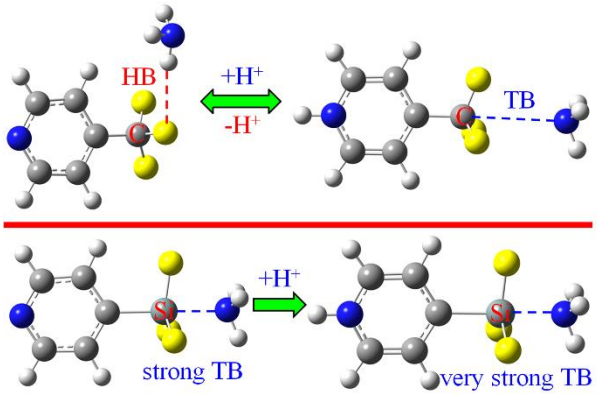

Protonation not only changes the primary interaction mode between α/β-furanCF_3/*p*-PyCF_3 and NH_3 but also prominently enhances the strength of Si/Ge···N tetrel bond.